Received: 6 October 2019 | Revised: 16 November 2019 | Accepted: 29 November 2019

DOI: 10.1002/aoc.5449

FULL PAPER

Applied Organometallic Chemistry WILEY

Copper iodide nanoparticles-decorated porous polysulfonamide gel: As effective catalyst for decarboxylative synthesis of *N*-Arylsulfonamides

Sedigheh Alavinia[1] | **Ramin Ghorbani-Vaghei**[1] | **Jamshid Rakhtshah**[2] | **Jaber Yousefi Seyf**[3] | **Iman Ali Arabian**[1]

[1]Department of Organic Chemistry, Faculty of Chemistry, Bu-Ali Sina University, 65174, Hamedan, Iran

[2]Department of Inorganic Chemistry, Faculty of Chemistry, University of Tabriz, Tabriz, Iran

[3]Department of Chemical Engineering, University of Technology, Hamedan, Iran

Correspondence
Ramin Ghorbani-Vaghei, Department of Organic Chemistry, Faculty of Chemistry, Bu-Ali Sina University, 65174, Hamedan, Iran.
Email: rgvaghei@yahoo.com

A porous cross-linked poly (ethyleneamine)-polysulfonamide (PEA-PSA) as a novel organic support system is synthesized in the presence of silica template by nanocasting technique. The paper demonstrates immobilization of CuI nanoparticles inside the pores (PEA-PSA@CuI) for the facile recovery and recycling of these nanoparticles. The presence of porous PEA-PSA and PEA-PSA@CuI nanocomposites was confirmed using FT-IR spectroscopy, FE-SEM, EDX, TGA, XRD, TEM, BET, XPS, WDX, ^{1}H NMR, and ICP-OES techniques. The PEA-PSA@CuI along with Ag(I)/$K_2S_2O_8$ was implemented as a reusable cooperative catalyst-oxidant system in the *N*-arylation of *p*-toluenesulfonamide with substituted carboxylic acids in mild condition. So, the novel decarboxylative cross-coupling catalyzed by copper and silver has been developed. Aromatic, secondary and tertiary aliphatic acids underwent high efficient decarboxylative processes with *p*-toluenesulfonamide to afford the corresponding products. This method provides a practical approach for the flexible synthesis of sulfonamides from the readily affordable substrates. The catalyst is highly reusable and efficient, especially in terms of time and yield of the desired product.

KEYWORDS

C-N coupling, Cross-linked polysulfonamide, Decarboxylative, Heterogeneous, Porous

1 | INTRODUCTION

Owing to the recent advances in *N*-arylation coupling reactions through transition metal catalysis, several effective methods have been proposed for the selective bond formation of carbon-heteroatom.[1–3] In this regard, *N*-Arylsulfonamides have various antibacterial,[4] antitumor,[5] and anti-HIV biological activities.[6] Aryl halides and aryl boronic acids can produce various products as primary substrates in the presence of strong bases or harsh reaction conditions.[7,8] Carboxylic acids are among the widely used coupling partners because of their abundance in nature as very sensitive organometallic reagents. Other advantages of these acids are their facile handling, the release of CO_2 as the waste product, and high regioselectivity at the carboxylic acid position in comparison to C–H.[9]

Decarboxylation of carboxylic acids is a promising coupling partner in organic synthesis. These acids are very useful in creating a bond between an aryl ring and a heteroatom generating similar organometallic intermediates followed by decarboxylation in organic synthesis.[10] In this regard, strategies such as Minisci reactions and Hunsdiecker decarboxylation are among the most

important decarboxylations interactions with silver salts.[11,12] Nevertheless, the Hunsdiecker protocol has a moderate yield and narrow reaction scopes and requires anhydrous silver salts.[13] The Minisci reaction is one of the most effective approaches for functionalization of electron-poor heterocycles.[14–16] Because of the interesting properties of silver(I) salts and its oxidant complexes, they are widely used in producing carbon and heteroatom-centered radicals.[17] Traditionally, the combination of peroxydisulfate and silver(I) has been applied in the Minisci reaction for organic synthesis. This method provides an efficient and direct means to substitute (hetero) arene compounds such as acylation, arylation and fluorination.[18] Although these precursors have numerous advantages, it is still difficult to design new protocols from them for dealing with the mentioned issues. Hence, designing new protocols for decreasing the use of additives, toxic reaction media, and homogeneous or expensive catalysts is still a challenging issue.

Gels are three-dimensional networks of cross-linked polymers built based on the molecular structure that can absorb different solvents. Cross-linking is considered as an important class of procedures because of its promising role in the modification of polymer networks and three-dimensional extensions of polymeric structures.[19,20] New gel structures fabricated using organic material *via* templates have recently attracted the attention of many researchers. The chemical synthesis procedure with the incorporation of template synthesis and self-organization can be used for structuring materials with extension scales. These materials have found great use in the primary and applied research such as sorbents for the adsorption of gas and the removal of organic compounds from water.[21] Owing to the attractive properties arising from the specific features of both polymers and porous gels, design and synthesis of new porous polymer gels have received considerable attention. The functional porous polymers are fabricated at a molecular level by controlling the surface area and applying a superior pore topology. Major techniques applied for preparation of new porous structures are nanocasting method, block copolymer self-assembly, and direct synthesis.[22] Among these techniques, combining self-assembly with the nanocasting methods have shown a high potential for the direct replication of the inverse structure of the preformed templates. These pathways use hard templates to create porous polymers that can incorporate several chemical functionalities at the pore surface.[22] Compared with metals and inorganic species, polymeric supports are excellent candidates for the design of powerful catalysts because of their ease of handling and processing.[23] The coating of the polymer structure is usually incomplete. In addition, the arrangement of the NPs is irregular.[24] To avoid these limitations and develop new methods for the synthesis of composite porous structures, the exploration of novel methodologies that control these parameters is still ongoing. Development of application of sulfonamide in coordination chemistry, medicinal chemistry, and catalytic fields has attracted the interest of many researchers.[25] Porous polysulfonamides are prepared from polymerization on the surface of silica template. The surfaces of porous cross-linked polysulfonamides must be modified using the transition metal precursors such as copper, which introduces new properties and applications (Figure 1).[26] CuI NPs have received a great deal of attention owing to their unique characteristics including nanometric size, large surface area, and better yields of products, particularly in multi-component reactions.[27] Thus, the use of porous cross-linked polysulfonamide as new support for the stabilization of CuI NPs for designing a new applied organometallic catalyst bearing both active Lewis acid and porous sites is an essential task for organic chemists. Despite reported copper-catalyzed couplings of sulfonamides with aryl

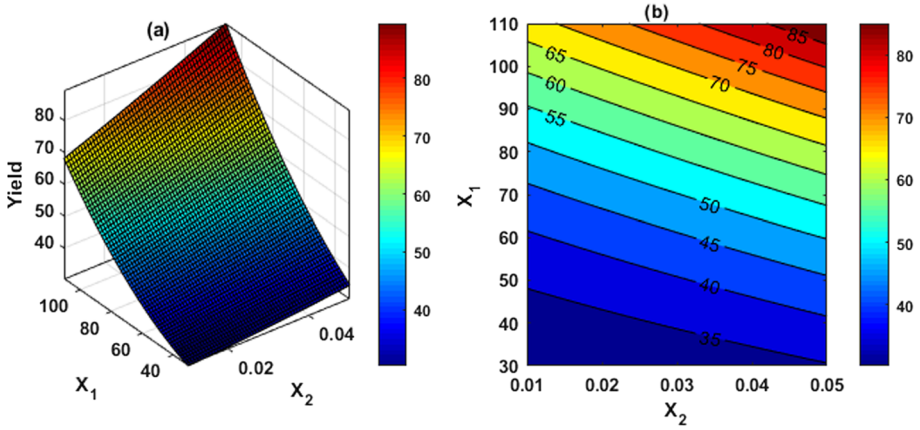

FIGURE 1 a) Three dimensional, and b) the contour of the reaction yield versus temperature and amount of the catalyst

halides by Wu[28] and Buchwald,[8] these reactions occur under harsh reaction conditions and at high temperatures.[29] Another important problem is the need for stoichiometric amount of metal catalyst and using arene carboxylic acids, which restricts their potential application. Therefore, the development of decarboxylative couplings that are capable of coupling alkyl carboxylic acids in a catalytic manner is of great necessity. In the present study, considering the interesting properties of the porous polymer-based catalysts and pursuing our recent study on porous materials as catalysts in multicomponent reaction,[30] we investigated the synthesis of a stable multifunctional catalyst bearing active Lewis acid groups (PEA-PSA@CuI). The PEA-PSA@CuI along with Ag(I)/$K_2S_2O_8$ was implemented as a reusable cooperative catalyst-oxidant system for selective arylation or alkenylation of *p*-toluenesulfonamide through decarboxylative cross-couplings of substituted aliphatic carboxylic acids (Scheme 1). Although polysulfonamide represents a potential application as a substrate in the field of the catalyst,[25] there is no report on the porous polysulfonamide or cross-linked polysulfonamide as a substrate in the area of the catalyst. Moreover, porosity, as a microstructured reactor, is a good characteristic to pre-concentrate substrates and enhance catalytically accessible active sites in order to increase reaction rate and product yield.[26] The other advantages of porous polysulfonamides as a catalyst support are included the low price of catalyst, easy to synthesis and the availability of monomers. The C-N coupling reaction could proceeds using catalytic amount of metals and both substrates are cheap and available.

2 | EXPERIMENTAL SETUP

2.1 | Chemicals and instruments

All commercially available chemicals were obtained from Merck and Fluka companies and used without further purification otherwise stated. Nuclear magnetic resonance (NMR) spectra were recorded in $CDCl_3$ on Bruker Avance spectrometers 250 MHz for ^1H NMR and 63 MHz for ^{13}C NMR using TMS as an internal standard; chemical shifts were expressed in parts per million (ppm). Infrared (IR) spectroscopy was conducted on a Perkin Elmer GX FT-IR spectrometer. Mass spectra were recorded on a Shimadzu QP 1100 BX Mass Spectrometer. Melting points were determined on a Stuarf Scientific SMP3 apparatus. Powder X-ray diffraction (PXRD) patterns recorded on a Rigaku XDS 2000 diffractometer using nickel-filtered CuKa radiation (λ =1.5418) over a range of <50°. Thermo-gravimetric analysis (TGA) was performed on a PYRIS DIAMOND instrument. Inductively coupled plasma-atomic emission spectroscopy (ICP-AES) was conducted on a Varian Vista MPX ICP-AES instrument. The sample was digested in conc. H_2SO_4: 30% aq. H_2O_2 (3:1 *v*/v) and heated until the solution became clear and colourless. The qualitative analysis of PEA-PSA@CuI was performed by using energy-dispersive X-ray spectroscopy (EDS). Scanning electron microscopy (SEM) was performed on EM3200 instrument operated at 30 kV accelerating voltage. For morphology observation, organogels that swell to equilibrium at 25 °C were freeze-dried in a freeze-dry system (LANCONCO) to remove ethanol completely. After drying, the gel samples were sputter coated with gold, and structures and morphologies of the gel surfaces were then visualized by a scanning electron microscope (Hitachi-X650). Transmission electron microscopy (TEM) was performed using a Zeiss-EM10C-100kv. Prior to the surface area analysis, the samples were activated in a high vacuum at 80 °C for 12 hr. All adsorption and desorption measurements were performed on a Micromeritics TriStar 3020 version 3.02 (N_2) system and measured at 77 K. The data were analyzed using the TriStar II 3020 V1.03 software (Micromeritics, Norcross, GA). The pore size distributions were calculated from the adsorption–desorption isotherms. Wavelength-dispersive X-ray spectroscopy (WDX) was performed using a TESCAN mira3. The chemical surface composition of the copper nanocomposite was determined by XPS (BesTec, Berlin, Germany).

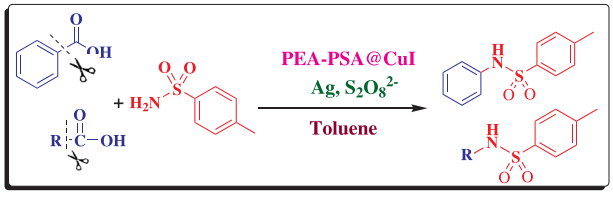

SCHEME 1 CuI/Ag-catalyzed decarboxylative C–N cross-coupling reaction

2.2 | Synthesis of Benzene-1,3-disulfonylchloride

PCl_5 (16.5 mmol), as chlorination agent, was added to the sodium salt of benzene-1,3-disulfonic acid (5.00 g, 18 mmol). To initiate the reaction, the vessel was heated (40–50 °C), then the reaction continues autonomously. After complete conversion (2 hr), crushed ice (100 g) and $CHCl_3$ (100 ml) was added and the organic layer was separated.[31]

2.3 | Synthesis of SiO_2 NPs

SiO_2 nanoparticles, with an average diameter of 20 nm, were synthesized in ethanol according to the Stöber method.[32] In summary, 100 ml ethanol, 21.6 ml deionized water, and 2.9 mL aqueous ammonia were added in a round bottom flask and stirred at ambient temperature for 10 min. Next, about 4.5 mL TEOS was slowly added to the solution by a syringe within 30 min and the reaction was kept on for 10 hr. The SiO_2 NPs were separated by centrifugation, rinsed with water and ethanol, then dried under vacuum conditions at 80 °C for 12 hr.

2.4 | Synthesis of SiO_2/PEA-PSA nanocomposite gel

The SiO_2 NPs (0.05 g) were treated with benzene-1,-3-disulfonyl chloride (1 mmol), ethane-1,2-diamine ($NH_2CH_2CH_2NH_2$) (0.7 mmol) and tris(2-aminoethyl) amine (N $(CH_2CH_2NH_2)_3$ (0.2 mmol) as follows: SiO_2 NPs was dispersed homogeneously in 30 mL of chloroform using the ultrasonication technique. After stirring at room temperature for 6 hr, a poly-sulfonamide silane-modified SiO_2 NPs (SiO_2/PEA-PSA NPs) gel was obtained. The gel was filtered off and washed with chloroform (20 mL) in triplicate and then dried under vacuum conditions at room temperature for 12 hr.

2.5 | Synthesis of porous PEA-PSA gel

The silica template of the silica@polysulfonamide nanocomposite prepared in the previous section was removed selectively through etching the SiO_2 NPs with an HF aqueous solution. 0.5 g of SiO_2/PEA-PSA NPs and deionized water (10 ml) were put in a plastic tube and sonicated for 5 min. Next, HF solution (30 ml, 5 wt%) was added into the mixture for 6 hr while magnetically stirring. The created porous gels were washed with ethanol, dried at 50 °C, and sieved through an 80 mesh screen.

2.6 | Synthesis of CuI NPs

CuI NPs were obtained by treating the solution of $CuSO_4$ (1 mmol) with the solution of KI (2 mmol) in 40 ml of distilled water. The solution of $CuSO_4$ was gradually submerged into a solution of KI and then sonicated for 30 min. The nanoparticles were separated, rinsed with water (2 × 25 ml), and dried.[33]

2.7 | Preparation of porous PEA-PSA@CuI gel

For loading CuI NPs, to an aqueous solution of CuI NPs in the H_2O (0.05 g in 20 ml), 0.1 g of the prepared polymeric support was added into the mixture for 12 hr while magnetically stirring. Afterward, the solid particles were separated, washed, with ethanol (2 × 25 mL) and water (2 × 25 mL) and dried at 50 °C. Finally, the porous PEA-PSA@CuI nanoparticles were collected, washed with water, separated through centrifugation, and dried under vacuum. The concentration of copper in the polymeric catalyst was 0.7 mmol/g determined by ICP-OES.

2.8 | Experimental design

The design of experiment (DOE), on the other hand, was used as a systematic approach to find the optimum reaction condition, including temperature and the amount of catalyst. Optimization shows that the optimum reaction conditions are 110 °C, and 0.05 g, for temperature and the amount of catalyst (PEA-PSA@CuI), respectively. The Central Composite Design (CCD), in summary, as an efficient response surface method in experimental design methodology was used to design the reactions to be carried out at laboratory. In our representative reaction (decarboxylative cross-coupling of benzoic acid with p-toluenesulfonamide), temperature (X_1) and the amount of catalyst (X_2) were chosen as the two main factors that would affect the reaction yield (Y). To investigate curvature in the reaction yield, three replicate at center point were applied, if there is one. The levels of the X_1 and X_2 and the corresponding response values (reaction yield) are given in Table 1. Analysis of variance (ANOVA) reveals that a quadratic model best fits to the experimental data. The analysis of variance is summarized in Table 2. The coefficient of determination (R^2) for the yield is 0.9997, which represents the good agreement between experimental reaction yields and yield obtained from quadratic model. The p-values imply that the model results are not due to chance. The smaller the p-value, the more the significant terms in the reaction yield.

Expression (1) shows the relation between representative reaction yield, temperature and the amount of the as-prepared catalyst:

$$Yield = 28.12 - 0.05X_1\text{-}106.09X_2 + 5.31X_1X_2 + 3.37 \times 10^{-3}X_1^2 + 986.84X_2^2 \quad (1)$$

Terms that have minus and plus sign, generally, have increasing and decreasing effect on the reaction yield,

TABLE 1 Levels of the experimental variables and the corresponding response values using the CCD method

	Independent variables		dependent variable
Runs	X_1 (temperature)	X_2 (amount of catalyst)	Yield (%)
1	30	0.03	32
2	70	0.03	50
3	70	0.05	56
4	30	0.05	35
5	110	0.01	68
6	70	0.03	50
7	30	0.01	30
8	70	0.03	50
9	70	0.01	44
10	110	0.03	78
11	110	0.05	90

TABLE 2 Analysis of variance (ANOVA) for the response surface quadratic model of the reaction yield

Source	p-val. Prob. > F
Model (yield)	<0.0001
X_1	<0.0001
X_2	<0.0001
X_1X_2	<0.0001
X_1^2	<0.0001
X_2^2	0.2539
R^2	0.9997
Predicted R^2	0.9969
Lack of fit	0.4000

respectively. The absolute magnitude of the coefficient in the equation (1) determines the extent of the effect. Figure 1 shows the 3 dimensional and the contour of reaction yield versus temperature and the amount of catalyst. As Figure 1 illustrates, increase in temperature and the amount of catalyst increase the reaction yield. All reactions in the optimization procedure, it should be emphasized, were ceased after 45 min. From theoretical point of view (Arrhenius equation), increasing the temperature, results increase in the reaction rate constant, which, in turn, leads to increase in reaction rate. It is then clear that the reaction yield increases at a specified time (45 min). By increasing the amount of catalyst, the number of effective collisions per unit volume increases, that is, the reaction yield increases.

2.9 | Optimization of reaction condition and validation of the model

To find out the optimum values of the temperature and the amount of catalyst, expression (1) together with numerical technique were used. Optimization showed that X_1 and X_2 should be equal to 110 °C and 0.05, respectively, which the reaction yield is equal to 89.55% in these conditions. Of more interest here is the predictive power of the proposed quadratic model. Accordingly, the representative reaction was carried out at optimum reaction conditions with three replicate. The mean value of obtained reaction yield is 90.00%. The deviation between experimental reaction yield and the yield obtained by the model is 0.50%. Very low deviation confirms the very well predictive power of the obtained model. Accordingly, the proposed quadratic model can be trusty used to obtain the reaction yield at each condition.

2.10 | General procedure for the synthesis of *N*-arylsulfonamides

At the obtained optimum reaction condition by the DOE, a mixture of carboxylic acid (1.2 mmol), $K_2S_2O_8$ (1 mmol) in toluene (0.5 mL), *p*-toluenesulfonamide (1 mmol), and silver nitrate (1 mol%, 2 mg) along with PEA-PSA@CuI (3.5 mol%, 0.05 g) was heated (110 °C, sealed tube). Once the reaction was completed, the solvent was evaporated and EtOAc (10 mL) was added to the mixture. Afterward, the nanocatalyst was eliminated by centrifugation, washed with acetone and water for several times, and dried at 60 °C for 3 hr. In the next step, water (100 mL) was added and extracted with EtOAc (30 mL) in triplicate. To obtain the desired sulfonamide, the organic layer was dried over $MgSO_4$, filtered, and concentrated in vacuum.

2.11 | Gel content

About 0.5 g of the sample (W_i) was placed in water for 24 hr at room temperature. The swollen part was separated by centrifugation and dried in a vacuum oven at 40 °C for 24 hr. Eventually, the samples were weighed (W_f). Here, the gel content (Gel (%)) is defined by Equation (1):

$$\text{Gel (\%)} = W_i/W_f * 100 \quad (1).$$

2.12 | Analytical data of selected products

N-phenyl-4-methyl-benzenesulfonamide: **(compound 3a).**

Known compound; mp: 111–112 °C (Lit. mp 109–112 °C)[34]

N-(p-tolyl)-4-methyl-benzenesulfonamide: **(compound 3b).**

Known compound; mp: 101–103 °C (Lit. mp 97–99 °C)[34]

N-(4-methoxyphenyl)-4-methylbenzenesulfonamide: **(compound 3c).**

Known compound; mp: 113–114 °C (Lit. mp 112–114 °C)[34]

N-(4-chlorophenyl)-4-methylbenzenesulfonamide: **(compound 3d).**

Known compound; mp: 119–122 °C (Lit. mp 119–122 °C)[34]

N-(4-nitrophenyl)-4-methylbenzenesulfonamide: **(compound 3e).**

Mp: 189–191 °C, IR (KBr): 3335, 1339, 1183 cm^{-1}. ^1H NMR (250 MHz, DMSO-d_6) δ 8.12 (d, J = 8.8 Hz, 2H), 7.77 (d, J = 7.9 Hz, 2H), 7.37 (d, J = 8.3 Hz, 2H), 7.32 (d, J = 7.9 Hz, 2H), 2.51 (s, 1H), 2.32 (s, 3H). ^{13}C NMR (63 MHz, DMSO-d_6) δ 144.79, 144.50, 142.94, 136.62, 130.43, 127.23, 125.78, 118.34, 21.41.

N-(2-nitrophenyl)-4-methylbenzenesulfonamide: **(compound 3f).**

Mp: 189–191 °C. IR (KBr): 3258, 1314, 1159 cm^{-1}. ^1H NMR (250 MHz, DMSO-d_6) δ 10.21 (s, 1H), 7.91 (d, J = 8.1 Hz, 1H), 7.63 (m, 3H), 7.37 (d, J = 8.0 Hz, 3H), 7.28 (d, J = 8.6 Hz, 1H), 2.51 (s, 3H). ^{13}C NMR (63 MHz, DMSO-d_6) δ 144.27, 143.35, 136.83, 134.67, 130.96, 130.24, 129.26, 127.32, 126.52, 125.94, 125.61, 21.45.

N-(naphthalen-1-yl) 4-methyl-benzenesulfonamide: **(compound 3 h).**

Mp: 155–157 °C, IR (KBr): 3296, 1303, 1142 cm^{-1}. ^1H NMR (250 MHz, Chloroform) δ 7.97–7.88 (m, 1H), 7.82 (d, J = 5.9 Hz, 1H), 7.70 (d, J = 8.2 Hz, 2H), 7.5–7.29 (m, 5H), 7.16 (d, J = 7.9 Hz, 2H), 2.34 (s, 3H). ^{13}C NMR (63 MHz, Chloroform) δ 143.76, 136.42, 134.25, 131.61, 129.56, 128.92, 128.35, 127.38, 127.11, 126.62, 126.27, 125.42, 122.61, 121.70, 21.51.

N-(4-chloro-3-nitrophenyl)-4-Methylbenzenesulfonamide: **(compound 3i).**

Mp: 162–164 °C. IR (KBr): 3232, 1372, 1138 cm^{-1}. ^1H NMR (250 MHz, Chloroform) δ 7.70 (d, J = 7.9 Hz, 2H), 7.45 (s, 1H), 7.27 (d, 2H, J = 8.3 Hz), 7.20 (d, J = 8.6 Hz, 2H), 7.06 (d, J = 8.4 Hz, 2H), 2.40 (s, 3H, CH_3). ^{13}C NMR (63 MHz, Chloroform) δ 144.24, 135.62, 135.30, 130.71, 129.82, 129.38, 127.32, 122.74, 21.56. Mass (m/z): 326.

N-(4-methyl-2-nitrophenyl) 4-ethylbenzenesulfonamide: **(compound 3j).**

Mp: 153–156 °C. ^1H NMR (250 MHz, Chloroform) δ 8.00 (d, J = 9.7 Hz, 2H), 7.87–7.56 (m, 2H), 7.31 (d, J = 8.9 Hz, 2H), 6.66 (d, J = 8.6 Hz, 2H), 4.13 (s, 1H, NH), 2.24 (s, 3H), 2.20 (s, 3H). ^{13}C NMR (63 MHz, Chloroform) δ 150.91, 130.06, 129.84, 127.85, 127.18, 126.64, 126.06, 124.09, 122.85, 120.00, 113.23, 17.67, 17.18.

N-(2-nitro-4-methoxyphenyl)-4-methylbenzenesulfonamide: **(compound 3k).**

Mp: 92–94 °C. IR (KBr): 3281, 1351, 1145 cm^{-1}. ^1H NMR (250 MHz, Chloroform) δ 9.26 (s, 1H), 7.75 (d, J = 9.2 Hz, 1H), 7.59 (d, J = 8.3 Hz, 2H), 7.46 (d, J = 3.0 Hz, 1H), 7.20 (d, J = 8.7 Hz, 2H), 7.15 (d, J = 3.0 Hz, 1H), 3.80 (s, 3H), 2.35 (s, 3H). ^{13}C NMR (63 MHz, Chloroform) δ 156.20, 144.63, 139.02, 135.49, 129.92, 127.09, 126.43, 124.62, 122.97, 109.16, 55.98, 21.54.

4-Methyl-N-(pyridin-2-yl)benzenesulfonamide: **(compound 3l).**

Known compound; Mp: 214–216 °C (Lit. mp 214–216 °C),[34] IR (KBr): 3229, 1356, 1140 cm^{-1}. ^1H NMR (250 MHz, Chloroform) δ 8.42 (s, 2H), 7.96–7.57 (m, 3H), 7.47 (s, 1H), 7.29 (s, 4H), 6.85 (s, 1H), 2.42 (s, 3H). ^{13}C NMR (63 MHz, Chloroform) δ 157.91, 148.73, 147.54, 144.53, 143.62, 134.18, 131.73, 120.92, 118.76, 26.24. Mass (m/z): 248.

4-Methyl-N-(pyrimidin-2-yl)benzenesulfonamide: **(compound 3m).**

Mp:203–205 °C, IR (KBr): 3119, 1360, 1168 cm^{-1}. ^1H NMR (250 MHz, Chloroform) δ 11.99 (s, 1H), 8.69 (d, J = 4.9 Hz, 2H), 8.03 (d, J = 8.0 Hz, 2H), 7.31 (d, J = 8.4 Hz, 2H), 7.01 (t, J = 5.0 Hz, 1H), 2.44 (s, 3H). ^{13}C NMR (63 MHz, DMSO) δ 158.58, 156.84, 144.16, 136.62, 129.30, 128.48, 115.76, 21.64. Mass (m/z):249.

N-(5-bromopyridin-2-yl)-4-methylbenzenesulfonamide **(compound 3n).**

Mp: 182–183 °C, IR (KBr): 3098, 1344, 1165 cm^{-1}. ^1H NMR (250 MHz, Chloroform) δ 10.95(s, 1H), 8.99 (s, 1H), 7.74 (dod, 10 Hz, 7.5 Hz, 2H), 7.40 (d, J = 7.5 Hz, 2H), 7.26 (d, J = 7.5 Hz, 2H), 2.42 (s, 3H). ^{13}C NMR (63 MHz, Chloroform) δ 150.19, 149.18, 144.33, 141.79, 136.37, 129.92, 127.12, 114.54, 113.41, 21.60. Mass (m/z):326.

N-(2,6-dichlorophenyl)-4-methylbenzenesulfonamide: **(compound 3o).**

Mp: 136–137 °C, IR (KBr): 3268, 1342, 1166 cm^{-1}. ^1H NMR (250 MHz, Chloroform) δ 7.79–7.65 (m, 1H), 7.28 (d, J = 7.8 Hz, 1H), 7.20 (d, J = 8.5 Hz, 1H), 7.08–6.94 (m, 1H), 2.42 (s, 1H). ^{13}C NMR (63 MHz, Chloroform) δ 144.61, 135.68, 134.56, 133.62, 130.13, 129.86, 127.28, 125.68, 122.92, 121.78, 21.61. Mass (m/z):316.

2-Methyl-N-tosylpropan-2-amine: **(compound 3p).**

Mp: 108–111 °C, IR (KBr): 3268, 1308, 1138 cm^{-1}. ^1H NMR (250 MHz, Chloroform) δ: 2.16 (s, 9H), 2.37 (s, 3H), 5.39 (d, J = 11.25 Hz, 1H), 7.24(d, J = 7.25 Hz, 2H),

7.68(d, J = 7.25 Hz, 2H). ^{13}C NMR (63 MHz, Chloroform) δ: 142.68, 140.63, 129.42, 126.92, 77.63, 77.12, 76.61, 54.39, 30.04, 21.45. Mass (m/z): 227.

N-cyclohexyl-4-methylbenzenesulfonamide: **(compound 3q).**

Mp:85–87 °C, IR (KBr): 3307, 1304, 1159 cm^{-1}. ^{1}H NMR (250 MHz, Chloroform) δ 1.11 (m, 5H), 1.44 (d, J = 7 Hz, 1H), 1.61 (m, 4H), 2.37 (s, 3H), 3.04 (s, 1H), 5.40 (d, J = 7 Hz, 1H), 7.24 (d, J = 6.25 Hz, 2H), 7.76 (d, J = 6.25 Hz, 2H). ^{13}C NMR (63 MHz, Chloroform) δ 142.98, 138.52, 129.57, 126.91, 52.53, 33.67, 25.09, 24.59, 21.46. Mass (m/z): 253.

2,3-Dihydro-N-tosylbenzo[b][1,4]dioxin-6-amine **(compound 3r).**

Mp: 193–195 °C, IR (KBr): 3239, 1301, 1158 cm^{-1}. ^{1}H NMR (250 MHz, DMSO-d_6) δ 2.28 (s, 3H), 4.10 (s, 4H), 6.51 (d, J = 8.5 Hz, 1H), 6.56 (s, 1H), 6.67 (d, J = 8.25 Hz, 1H), 7. 28 (d, J = 7 Hz, 2H), 7.57 (d, J = 7 Hz, 2H). ^{13}C NMR (63 MHz, DMSO-d_6) δ 143.51, 140.86, 137.09, 131.41, 130.04, 127.13, 117.66, 114.62, 110.44, 64.49, 64.23, 21.34. Mass (m/z): 305.

3 | RESULTS AND DISCUSSION

3.1 | Characterization of immobilized CuI NPs in porous nanocomposite as a heterogeneous catalyst

Figure 2 provides a schematic representation of the prepared catalyst. This heterogeneous catalyst was created through immobilization of CuI NPs in the structure of porous nanocomposite by complexation with numerous sulfonamide groups of PEA-PSA and absorbing in the pores.

The typical FT-IR spectra of SiO_2/PEA-PSA (a), porous PEA-PSA (b), and PEA-PSA@CuI (c) are shown in Figure 3. The characteristic peak of SiO_2 at 1112 cm^{-1} is ascribed to Si-O stretching vibrations of silica nanoparticles trapped in polymer chains.[35] This peak does not appear in the FT-IR spectra of the PEA-PSA and CuI@PEA-PSA (Figures 3b and 3c). In the spectrum of PEA-PSA, the absorption bands at 1334 and 1163 cm^{-1} are indexed to the S=O stretching vibrations (Figure 3b).[25] After the coordination of CuI nanoparticles to these situations, the S=O bonds shifted to lower wavenumber (i.e., 1327 and 1152 cm^{-1}) in the spectrum of the final product (Figure 3c). As can be inferred from these changes, the metal ions are coordinated with the oxygen donor atoms of the PEA-PSA as a ligand.

Figure 4 illustrates the XRD patterns of PEA-PSA@CuI. The appearance of peaks at 2θ = 25.6, 29.6,

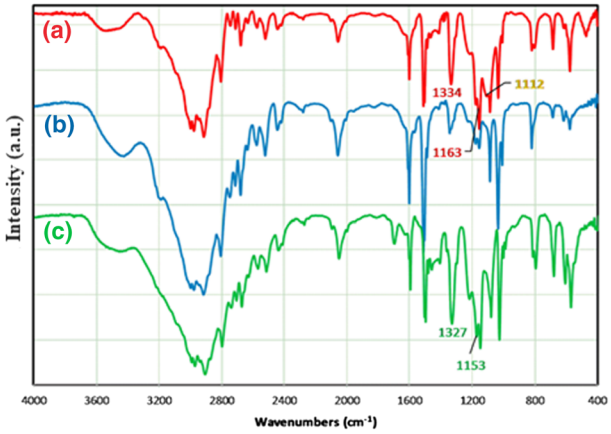

FIGURE 3 FT-IR spectra of SiO2/PEA-PSA (a), porous PEA-PSA (b), and PEA-PSA@CuI (c)

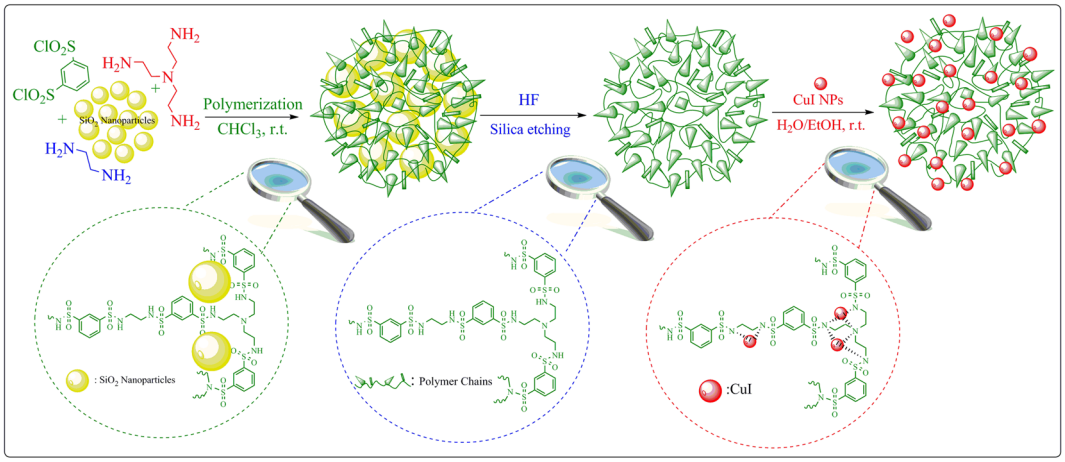

FIGURE 2 A sequence of events in the preparation of loaded CuI NPs in the structure of porous PEA-PSA nanocomposite gel

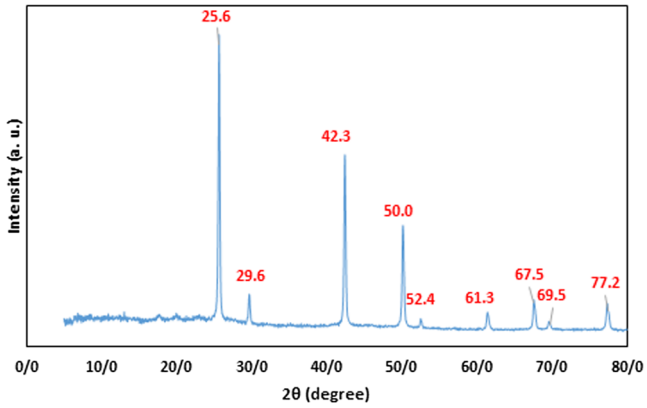

FIGURE 4 XRD patterns of PEA-PSA@CuI

42.3, 50.0, 52.4, 61.3, 67.5, 69.5 and 77.2° is attributed to CuI species of the catalyst.[33] The XRD patterns clearly confirm the coating of CuI NPs in PEA-PSA due to the diffraction peaks of CuI NPs. Also, the XRD pattern of PEA-PSA@CuI given in Figure 4 shows that SiO_2 NPs have been removed through the silica etching process.

To gain further information about obtained nanocomposite gels, we investigated its morphological characterizations with FE-SEM method. Figure 5 illustrates the SEM images of the crosslinked polymer (a), silica/PEA-PSA (b), and porous PEA-PSA (c-d). The cross-linked PEA-PSA gel showed a smooth and tight surface (Figure 5a). Figures 5c-d show SEM images of PEA-PSA gel obtained from SiO_2/PEA-PSA composites by the selective removal of silica NPs *via* a chemical etching. The figure also shows PEA-PSA layered structures with 3D porous structures. The removal of the template significantly affected the morphology of the PEA-PSA, probably due to the creation of porosity on the surface of the polymer. Cryo-scanning electron microscopy (Cryo-SEM) was applied to characterize porosity and internal morphology of freeze-dried porous PEA- PSA gel (Figure 5c and 5d). For this purpose, lyophilization was applied in order to induce pore structure into the PEA-PSA gel. Using liquid nitrogen, the solvent-swollen PEA-PSA gels were cooled rapidly. In the next step, to create a porous structure in the gel, the frozen solvent was removed through sublimation under vacuum behind voids. The obtained sample shows a uniform 3D porous network with a large number of pores. The surface of freeze-dried gel is very loose, which contributes to the diffusion of the solvent into or out of the gel structure during the swelling and deswelling of polysulfonamide gels.

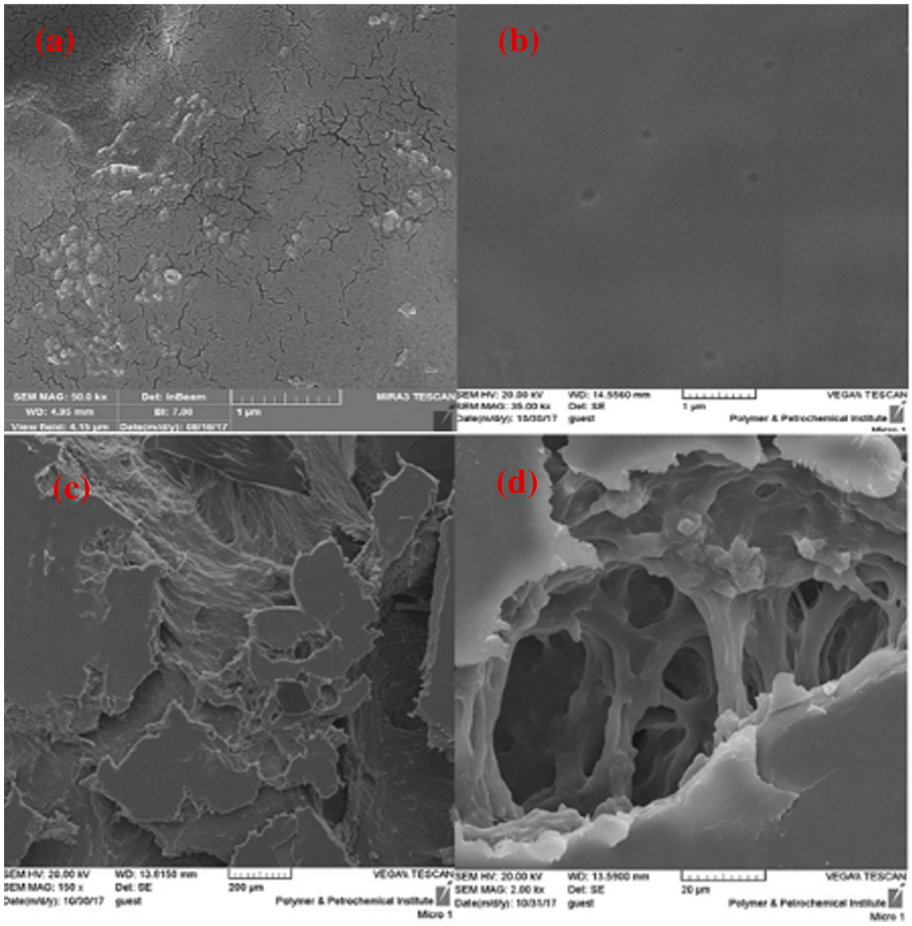

FIGURE 5 FE-SEM photographs of cross-linked PEA-PSA (a), SiO2/PEA-PSA (b), and freeze-dried porous PEAPSA gel (c-d)

This interconnected nanoscale matrix provides a higher porosity and active surface area in comparison to agglomerated nanoparticles.[36]

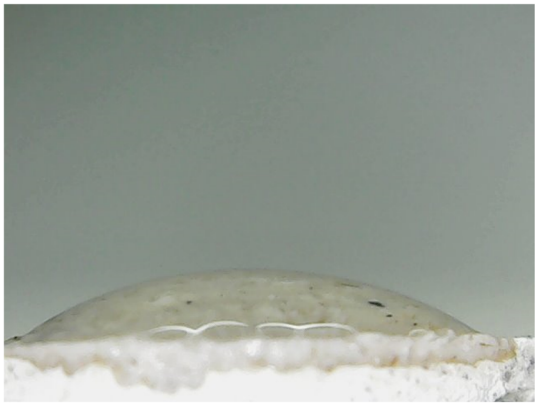

FIGURE 6 Contact angles of nanopure water droplets on PEMA-PSA

The wettability was examined *via* measuring the contact angle (CA). Figure 6 presents the CAs of water droplet sample. Based on the obtained results, the CA between water and polymers was less than 90°, which indicates a good hydrophilicity behavior.[37]

Figure 7 shows the morphology of PEA-PSA@CuI and CuI NPs as obtained by FE-SEM micrographs. The figures show a homogeneous nanostructure, proving that a nanoscale surface was obtained. Moreover, excellent dispersing of CuI NPs within the gel matrix and the presence of copper nanoparticles bonded to the organic matrix in the catalyst were confirmed. It is well known that PEA-PSA gel can encapsulate the nanoparticles in the pores and prevent their aggregation (Figure 7a).

Wavelength-dispersive X-ray spectroscopy (WDX) is an efficient method to generate qualitative data on the distribution of different chemical elements in the catalyst matrix. Elemental maps for the synthesized nanocatalyst are illustrated in Figure 8. As can be seen, C, N, S, O, I, and Cu are distributed homogeneously, confirming the

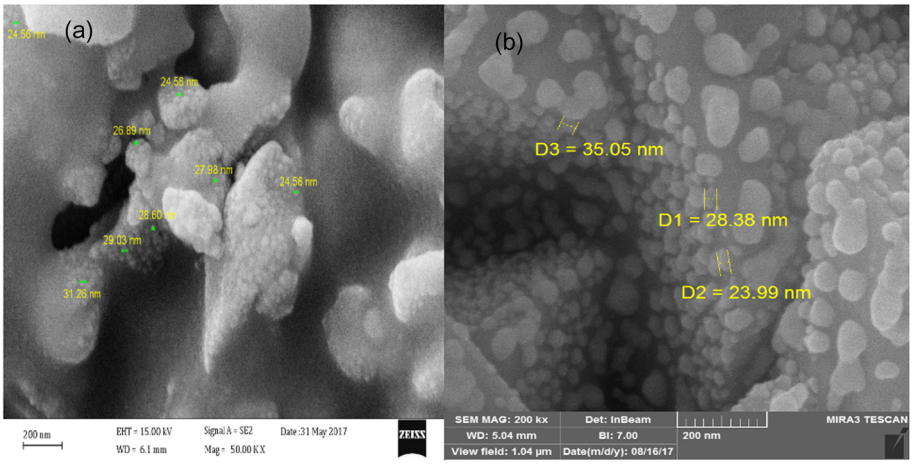

FIGURE 7 FE-SEM of PEA-PSA@CuI nanocomposite (a) and CuI NPs (b)

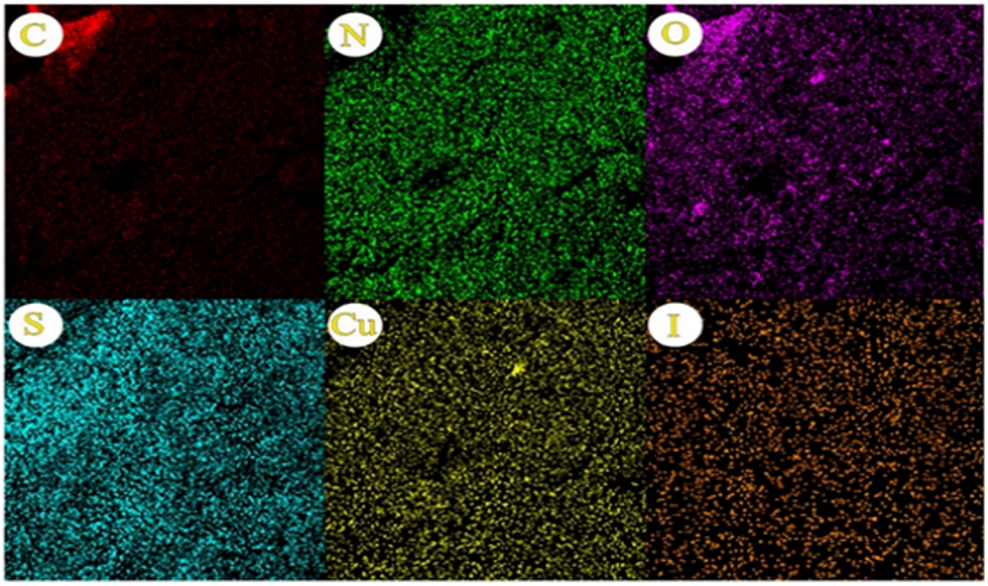

FIGURE 8 SEM image of PEA-PSA@CuI; which shows the presence of C, N, S, O, Cu and I atoms in the catalyst

uniform distribution of nanoparticles in the prepared sample.

After CuI NPs immobilizing in the matrix of PEA-PSA gel, the uniformly dispersed small CuI NPs was observed with approximate spherical shape in the TEM image (Figures 9a and 9b). As can be observed, CuI NPs distribution is controlled in the presence of PEA-PSA gel matrix.

ICP-OES analysis was performed to determine the exact amount of Cu loaded on poly (ethyleneamine)-polysulfonamide, which was found to be 0.7 mmol per gram of the catalyst. The high amount of the loaded copper NPs can be attributed to the gel nature of polymeric support as well as the presence of large chelating groups on the nanocomposite. Afterward, energy dispersive spectrometer (EDS) was applied to analyze the cross-linked PEA-PSA (a) and PEA-PSA@CuI (b). The EDS analysis of PEA-PSA@CuI (Figure 10 b) shows signals of carbon, oxygen, nitrogen, sulfur, iodine, and copper in the structure of the nanocomposite gel. The EDS analysis of PEA-PSA and PEA-PSA@CuI indicates that the Si atom was removed from the silica particles coated with PEA-PSA by the HF etching.

The Brunauer–Emmett–Teller (BET) surface area analysis was performed to estimate the specific surface area of PEA-PSA (Figure 11). The N_2 isotherm reveal the

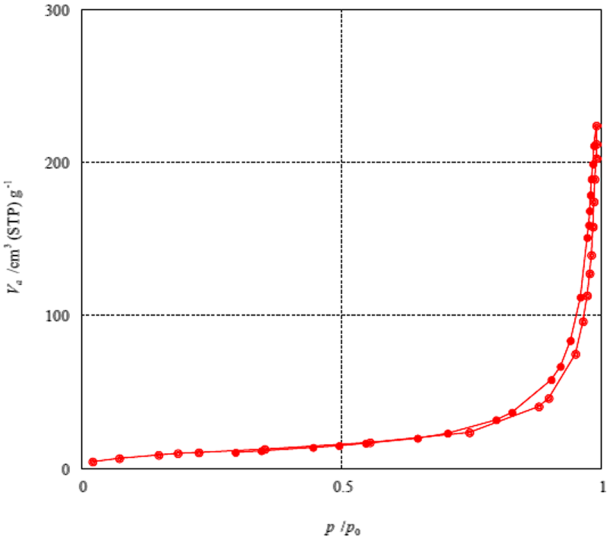

FIGURE 11 N2 adsorption–desorption isotherms and the corresponding pore size distributions for PEA-PSA

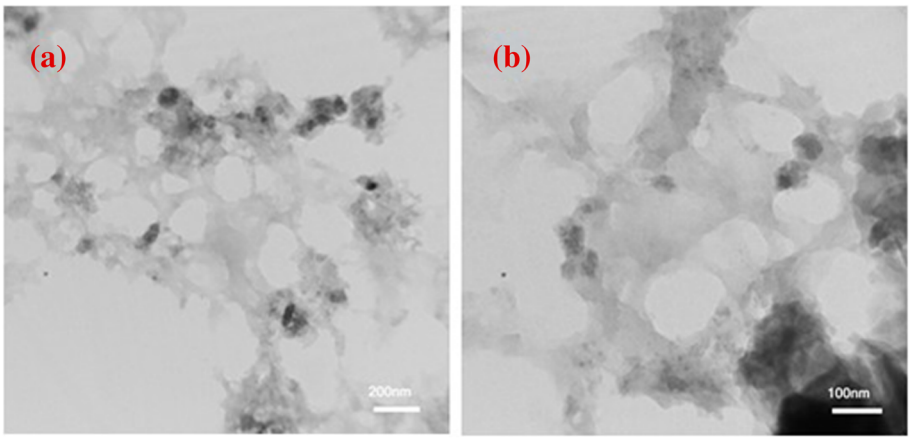

FIGURE 9 TEM images of PEA-PSA@CuI gel with the scale bar of 200 nm (a) and 100 nm (b)

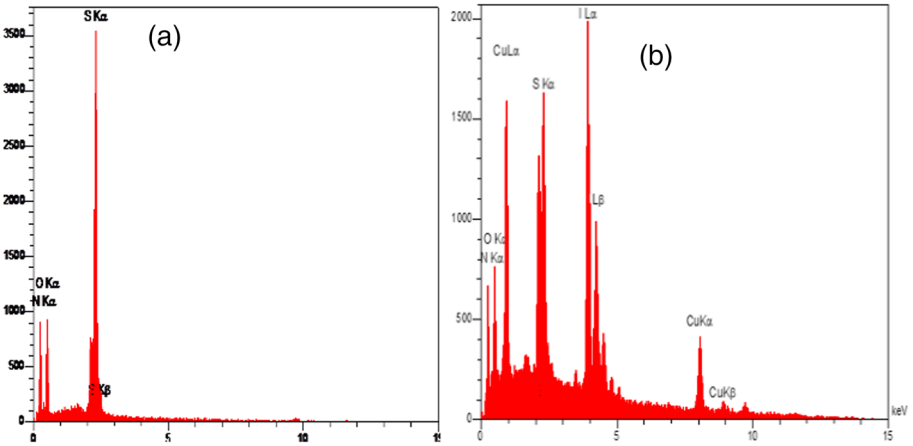

FIGURE 10 The comparison of EDS analysis of PEA-PSA (a) and PEA-PSA@CuI (b)

TABLE 3 Texture parameters obtained from nitrogen adsorption studies

Sample	SBET ($m^2\ g^{-1}$)	Pore diameter by BJH method (nm)	Pore volume ($cm^3\ g^{-1}$)
PEA-PSA	560	56.36	0.43

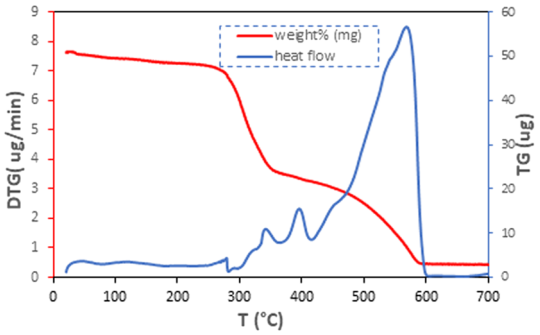

FIGURE 12 Thermogravimetric diagram of PEA-PSA@CuI

typical type IV isotherm with type H3 hysteresis (defined by IUPAC), which are identified as mesoporous materials. Table 3 summarizes the results of N_2 adsorption–desorption including pore diameters (DBJH), the BET surface area (SBET), and the total pore volume (V_{total}) of the studied samples. (Table 3).

TGA curve of PEA-PSA@CuI shown in Figure 12 was segmented into multiple regions with respect to the mass loss of the prepared samples. For organic solvents and physically absorbed water, a mass loss starting at 100 °C is observed. This mass loss at higher temperatures (250–350 °C) is majorly attributed to the loss of organic groups[25] from the polymeric structure. Additionally, polymer residue decomposition occurred at the third mass loss, within the temperature range of 350–600 °C.

The surface turnover of the PEA-PSA@CuI was investigated by XPS analysis. CuI existence in the PEA-PSA@CuI was re-confirmed by XPS analysis through studying binding energy (Figure 13a-b). Figure 13a-b show XPS spectra of Cu 2p and I 3d core level acquired

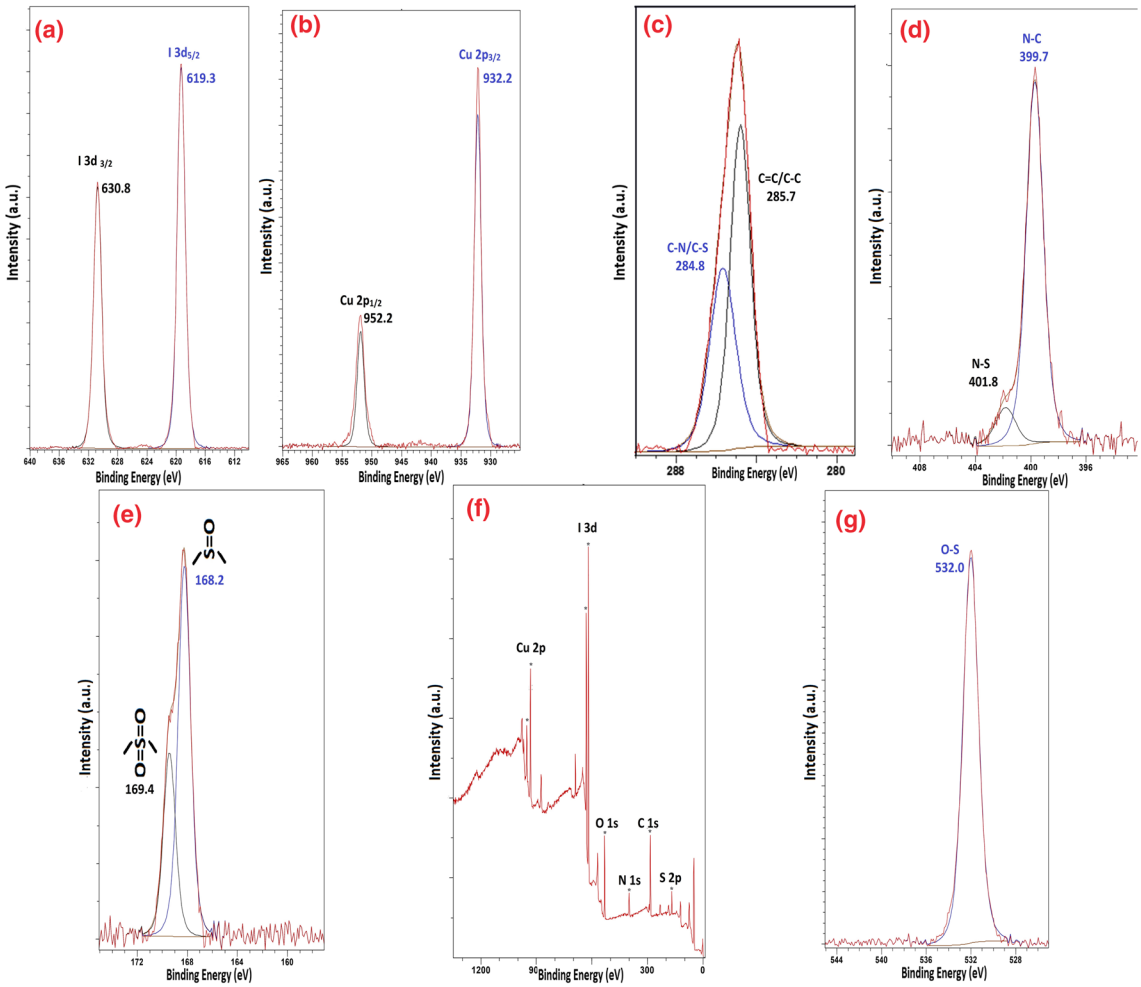

FIGURE 13 XPS spectra of PEA-PSA@CuI (a) I3d (b) Cu2p (c) C 1 s (d) N 1 s (e) S 2p (f????????) survey spectrum of PEA-PSA@CuI and (g) O 1 s

from an as-prepared sample. The peak positions of I 3d, 619.3 eV and 630.8 eV, are in good agreement with the literature data for CuI material[38] (Figure 13a). The positions of the peaks of Cu $2p_{1/2}$ and $2p_{3/2}$ of the sample are 952.2 eV and 932.2 eV, respectively, without the shake-up, which implies a feature of Cu^{+} (Figure 13b). The presence of C, N, S and O in PEA-PSA@CuI sample was confirmed by the characteristic peaks for C 1 s at binding energy (BE) of about 284.8 and 285.7 eV (Figure 13c), N 1 s at BE of about 399.7 and 401.8 eV (Figure 13d), and O1S at BE of about 532.0 eV (Figure 13g) and S 2P at 168.2 and 169.4 eV (Figure 13e). The peak consisting of 168.6 and 169.9 eV corresponds to -C-S(O)-C-sulfone bridges.[39] Here, the more area in the peak of 168.6 and 169.9 eV indicates that S atom exists as sulfone bridges which matches with the -S=O stretch in IR at 1095 cm^{-1}. In addition, the characteristic peaks for O1s included three peaks at 352.0 eV (S–O bonding) indicating that the CuI NPs was successfully introduced onto the PEA-PSA surface by bond linkages (Figure 13e). The position of C 1 s peak is frequently affected by the local chemical/physical environment around it, and its area showed two type of nitrogen. The elemental peaks are dominated by O, S, N, Cu, I and C of nanocomposite gel (Figure 13f). It can be concluded that PEA-PSA have a variety of polar groups including alkyl, amine, and sulfonyl. The characteristic peaks related to silica (Si 2p) is not visible in the XPS elemental survey indicated that the Si atom was removed from the silica particles coated with polysulfonamide by the HF etching. Based on the XPS analysis, a possible structure of PEA-PSA@CuI is given in the Figure 2.

3.2 | CuI immobilized in poly (ethyleneamine)-polysulfonamide nanocomposite catalytic activity

In this section, the catalytic effect of PEA-PSA@CuI and PEA-PSA@Ag nanocomposite as a catalyst was investigated in the synthesis of 4-methyl-*N*-phenyl benzenesulfonamide 3a as a model compound. We chose the decarboxylative cross-coupling between benzoic acid (1a) and *p*-toluenesulfonamide (2a) as a model reaction commonly used in optimization studies (Table 4). Initially, the catalytic activity of $AgNO_3$ and PEA-PSA@Ag was investigated for the synthesis of 3a. The best result was obtained when using 6 mol% of PEA-PSA@Ag, which gives 3a in 30% yield (entry 4). Then, we evaluated the effect of the effect of CuI NPs on the model reaction progress. According to Table 4, in the presence of 20 mol% CuI NPs along with PEA-PSA@Ag, the yield of the reaction was increased to 45% (entry 6). In the next step, the effect of PEA-PSA@CuI was investigated and 3.5 mol% of the nanocomposite was the optimal amount to this reaction and giving 3a in 72% yield (entry 8). Also, the reaction was tested using CuI salt as the catalyst, but, in comparison with the prepared catalyst, the obtained data were not satisfactory and the PEA-PSA@ CuI shows better performance than CuI salt (6 hr, 50%). Increasing the amount of CuI/PEA-PSA has no significant effect on the reaction progress (entry 9). Then, the effect of $AgNO_3$ along with PEA-PSA@CuI was examined and the coupled product yield was improved (1 hr, 90%) (entry 10). Furthermore, the effect of different solvents was investigated. The addition of EtOH, H_2O, CH_3CN to the reaction system declined the yield of 3a (entries 17–21) and the best result was obtained in toluene (entry 10). Here, the oxidant has an important role in this reaction. In this study, the reaction did not take place in the absence of persulfate under O_2 atmosphere (entry 14). When the amount of $K_2S_2O_8$ was 0.5 equivalents, the yield of the reaction dropped to 45% (entry 13). By using one equivalent $K_2S_2O_8$, the yield increased up to 90%. Also we examined the effect of different oxidants including benzoyl peroxide and $(NH_4)_2S_2O_8$ on the progress of the reaction and the yields of 3a dropped (entries 15–16), followed by studying the efficacy of $AgNO_3$ on the reaction progress. To our surprise, increasing the $AgNO_3$ to 2 mol% decreased the product yield (entry 12), whereas decreasing the $AgNO_3$ concentration to 1 mol% increased the yield. Different bases such as K_3PO_4, Et_3N, K_2CO_3, and KOH were applied in this transformation and found that the reaction in the presence of different bases leads to reduction in efficiency.

These results motivated us to examine various aspects and generality of this approach for different aromatic carboxylic acids under optimized conditions. According to Table 5, a broad substrate scope is observed for both electron-donating and electron-withdrawing substituents such as nitro (**3e**, **3f**, **3i**, **3j**, **3 k**), methyl (**3b**, **3 g**, **3j**), chloro (**3d**, **3i**, **3o**), bromo (**3n**), methoxy (**3c, 3k**), as well as heterocyclic carboxylic acids such as picolinic acid, pyrimidine-2-carboxylic acid and 5-bromopicolinic acid (**3l**, **3m**, **3n**), and aliphatic carboxylic acids (**3p**, **3q**). Overall, these acids provided the desired cross-coupling products with good to excellent yields. As can be noticed, due to the difference in decarboxylation rates, the efficiency of the decarboxylative cross-coupling reaction is influenced by substituents. For instance, in comparison to para-chloro-substituents, benzoic acids containing a para-nitro substituent provided more desired results (**3d** vs. **3e**). Also, it was observed that substituted carboxylic acids containing electron-withdrawing groups (e.g., nitro and halogen) reacted faster than carboxylic acids containing electron-donating groups. Moreover, substituted

TABLE 4 Optimizing the reaction conditions for decarboxylative cross-coupling of benzoic acid with *p*-toluenesulfonamide reagent[a]

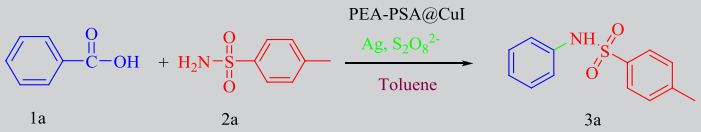

Entry	Cat. (mol%)	Oxidant (eq)	Solvent/Time (h)	3a (%)
1	$AgNO_3$ (5)	$K_2S_2O_8$ (1)	10/Toluene	10
2	$AgNO_3$ (10)	$K_2S_2O_8$ (1)	10/Toluene	12
3	PEA-PSA@ Ag (3)	$K_2S_2O_8$ (1)	Toluene/10	28
4	PEA-PSA@ Ag (6)	$K_2S_2O_8$ (1)	Toluene/10	30
5	PEA-PSA@ Ag (12)	$K_2S_2O_8$ (1)	Toluene/10	30
6	PEA-PSA@Ag (6), CuI NPs (10)	$K_2S_2O_8$ (1)	Toluene/5	45
7	PEA-PSA@Ag (6), CuI NPs (20)	$K_2S_2O_8$ (1)	Toluene/5	55
8	PEA-PSA@CuI (3.5)	$K_2S_2O_8$ (1)	Toluene/2	72
9	PEA-PSA@CuI (7)	$K_2S_2O_8$ (1)	Toluene/2	70
10	$AgNO_3$ (1), PEA-PSA@CuI (3.5)	$K_2S_2O_8$ (1)	Toluene/1	90
11	$AgNO_3$ (1), PEA-PSA@CuI (7)	$K_2S_2O_8$ (1)	Toluene/1	89
12	$AgNO_3$ (2), PEA-PSA@CuI (3.5)	$K_2S_2O_8$ (1)	Toluene/1	87
13	$AgNO_3$ (1), PEA-PSA@CuI (3.5)	$K_2S_2O_8$ (0.5)	Toluene/1	45
14	$AgNO_3$ (1), PEA-PSA@CuI (3.5)		Toluene/1	0[b]
15	$AgNO_3$ (1), PEA-PSA@CuI (3.5)	Benzoylperoxide (1)	Toluene/1	27
16	$AgNO_3$ (1), PEA-PSA@CuI (3.5)	$(NH_4)_2S_2O_8$ (1)	Toluene/1	35
17	$AgNO_3$ (1), PEA-PSA@CuI (3.5)	$K_2S_2O_8$ (1)	EtOH/1	10
18	$AgNO_3$ (1), PEA-PSA@CuI (3.5)	$K_2S_2O_8$ (1)	CH_3CN/1	15
19	$AgNO_3$ (1), PEA-PSA@CuI (3.5)	$K_2S_2O_8$ (1)	DMF/1	55
20	$AgNO_3$ (1), PEA-PSA@CuI (3.5)	$K_2S_2O_8$ (1)	DMSO/1	60
21	$AgNO_3$ (1), PEA-PSA@CuI (3.5)	$K_2S_2O_8$ (1)	H_2O/1	0[b]

[a]Reaction conditions: **1a** (1 mmol), **2a** (1.2 mmol), PEA-PSA@CuI (3.5 mol%), $AgNO_3$ (1 mol%), $K_2S_2O_8$ (1 mmol), toluene (0.5 ml), 110 °C, sealed tube
[b]The reaction was not occurred.

carboxylic acids like picolinic acid, pyrimidine-2-carboxylic acid, and 5-bromopicolinic acid, which are able to stabilize high-valent silver species,[40] participate in the decarboxylative cross-coupling reaction and gave reasonable yields. In this protocol, the position of the substituent affects the progress of the reaction. Benzoic acids bearing para-substituents provided larger yields compared to benzoic acids containing ortho substituents (**3e** *vs.* **3f**). Notably, we successfully synthesized new sulfonamides using 2,3-dihydrobenzo[b] [1,4] dioxin-6-carboxylic acid, which has not been reported elsewhere (**3r**). Afterward, we extended this protocol to the coupling of alkyl carboxylic acids with *p*-toluenesulfonamide. Both tertiary and secondary aliphatic acids (**3q** and **3p**, respectively) were subjected to high-efficiency decarboxylative-coupling processes with *p*-toluenesulfonamide to obtain the corresponding products in excellent yields. Carboxylic acid derivatives containing aromatic groups were better substrates compared with tertiary and secondary carboxylic acids.[41] Primary acids, on the other hand, failed to proceed under current conditions. The reaction of *p*-aminobenzoic acid also was examined and found that the reaction could not proceed even after prolonged reaction time. This method was highly high selective for the products. All products were examined using their spectroscopic data such as MS, IR, ^{13}C NMR, and ^{1}H NMR.

3.3 | Proposed reaction mechanism

To gain mechanistic insights, additional experiments were performed. When, the reaction was conducted in

TABLE 5 Decarboxylative cross-coupling of benzoic acids with *p*-toluenesulfonamide

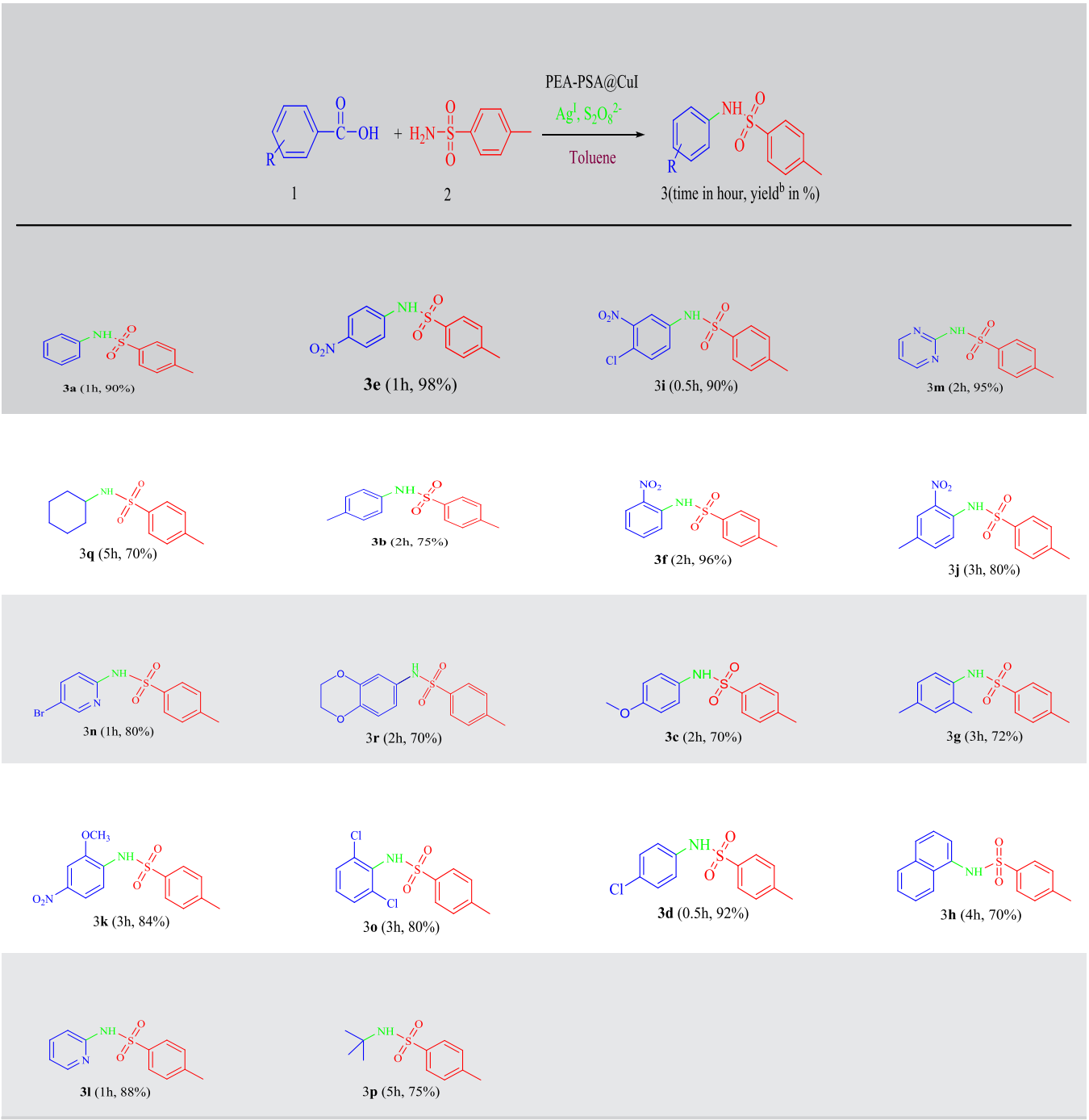

[a]Reaction condition: **1** (1.2 mmol), **2** (1 mmol), silver(I) salt (1 mol%), $K_2S_2O_8$ (1 mmol), PEA-PSA@CuI (3.5 mol%), toluene (0.5 ml), 110 °C, sealed tube,
[b]Isolated yield.

the presence of radical scavengers, such as 2,6-ditert-butyl-4-methylphenol (BHT), none of decarboxylative cross-coupling products were observed. This result suggests that the reaction may involve a radical pathway (Scheme 2).

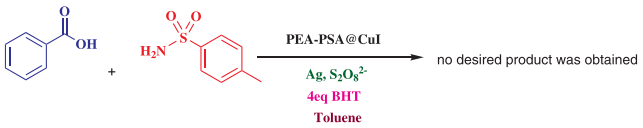

SCHEME 2 Radical Scavenger Experiment

The proposed reaction mechanism in the presence of PEA-PSA@CuI and silver(I)/persulfate is presented in Scheme 3. It is suggested that copper(I) decarboxylates the carboxylic acid and produces the aryl radical.[17] We believed Ag (II) along with Cu (II) can be facilitate the

SCHEME 3 Possible reaction mechanism of N-arylation of p-toluene sulfonamide with different substituted carboxylic acids

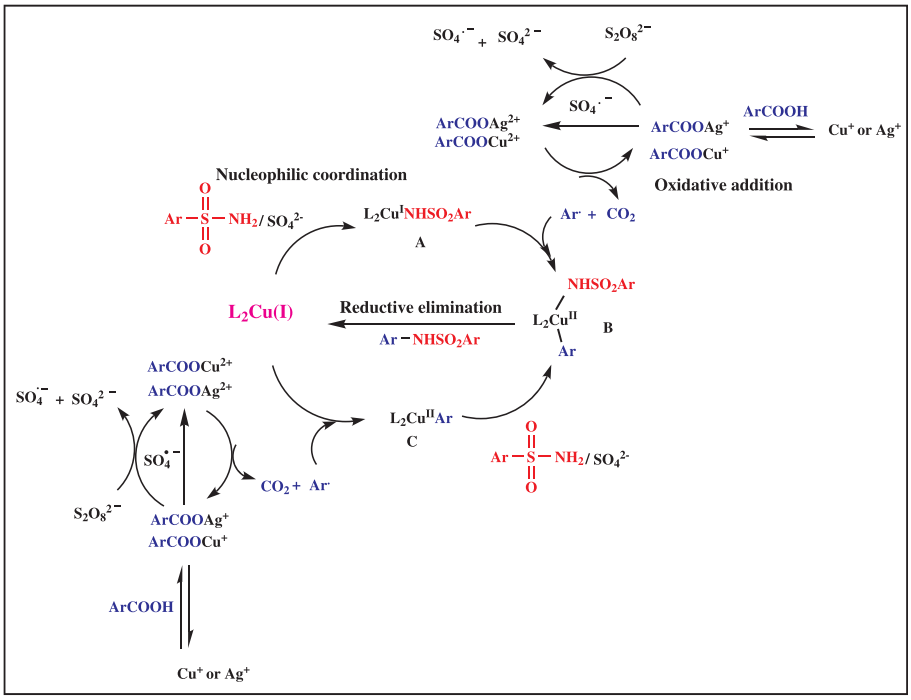

produce of aryl radical by the assistance of potassium persulfate. Because in the absence of $AgNO_3$ the yield of the product was decreased. Also, aromatic ring in carboxylic acid is very important because it could stabilize the benzyl radical and help the intermediate to finish the decarboxylative step fast and the final products are relatively stable under the oxydic conditions. The radical subsequently undergoes a substitution step with sulfonamides to form the final product. As can be seen, initially, in the nucleophilic coordination step, the sulfonamide used throughout the reaction with base generates the deprotonated nucleophile species and the sulfonamide coordinates to Cu(I) forming complex intermediate **A**. Subsequently, the silver(I) and copper (I) decarboxylate carboxylic acid leading to an aryl radical generation.[18] After oxidation of Cu(I) to Cu (II), the aryl group transfers to copper species (**A**) and results in the formation of intermediate **B**. Eventually, reductive elimination of intermediate **B** leads to the desired product and regenerates the catalyst (Scheme 3). In another mechanistic pathway, the intermediate C through an oxidative addition of aryl radical and Cu-based catalyst is generated, and the second coordination process gives the Cu (II)-based complex B. Finally, reductive elimination process of intermediate B yields the desired products and regenerates the catalyst. It is worth mentioning that compared with cross-coupling reactions catalysed by Pd(0), the oxidative addition step occurs before the trans metalation step. But in the copper catalysed cyclic system both of the routes of Scheme 3 are acceptable (due to the unpredictability of the relative order of these two steps).[40,42]

3.4 | Catalyst recycling

Once the reaction was completed, the catalyst was recovered by washing with acetone and water and then oven-dried at 50 °C to be used for six times. The reusability and catalytic activity of PEA–PSA@CuI were tested for about six consecutive cycles for the synthesis of 4-methyl-*N*-phenylbenzenesulfonamide **3a**. The results revealed a small activity loss even after six cycles (90, 88, 88, 88, 86, and 84 respectively). This observation proves that there was negligible Cu leaching from the polymeric supported system, which promotes reusability of the CuNPs. To determine the exact extent of Cu leaching, ICP-OES analysis was used, which detected only negligible Cu leaching (<0.08 ppm) in solution after the 6th run. Consequently, the CuNPs remained active in repetitive catalytic cycles due to excellent stabilization of Cu species by the porous polysulfonamid matrix. The SEM images of the catalyst before and after the reaction revealing the maintenance of the morphology with nanometric dimensions after the reaction. The FT-IR analysis of recycled catalyst showed the stability of the PEA-PSA@CuI during the recycling procedure (Figure 14).

3.5 | Efficiency comparison of the catalytic activity

According to the literature, different methods are utilized for the synthesis of *N*-arylsulfonamides *via* metal-catalyzed cross-coupling of sulfonamides with either aryl boronic acids or acids aryl halides (Scheme 4,

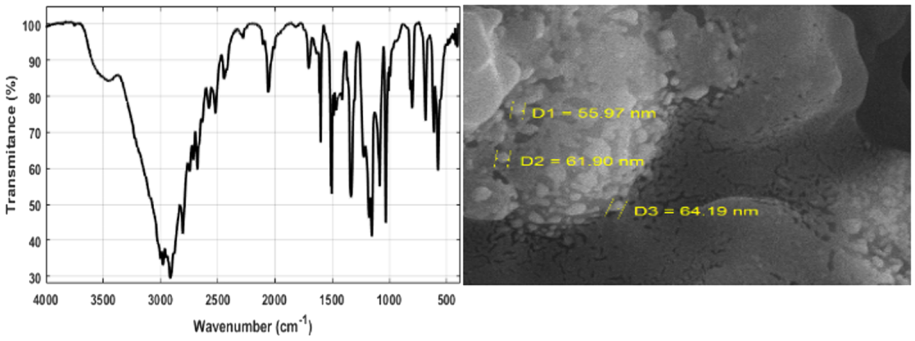

FIGURE 14 FT-IR spectra and SEM images of PEA-PSA@CuI after the reaction

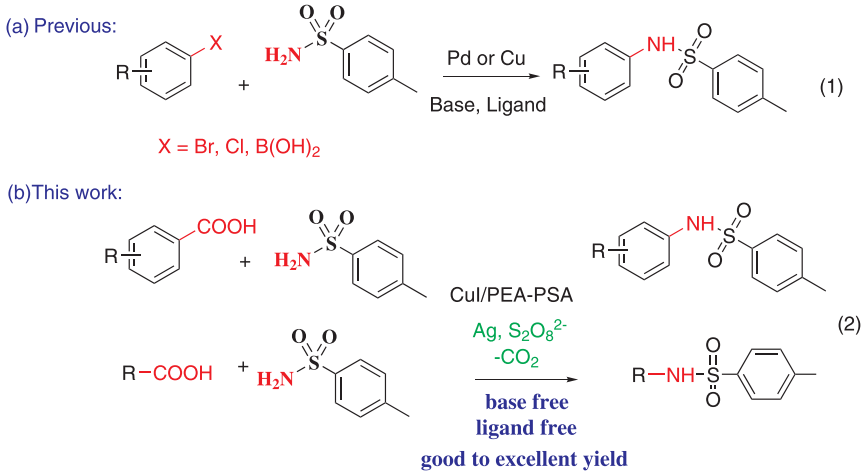

SCHEME 4 Various methods for synthesis of N-arylsulfonamides

equation (1)). As shown in Table 6, palladium and copper are applied as catalysts under different conditions. It is of note that, in the current work, using PEA-PSA@CuI along with the silver(I)/persulfate can remarkably shorten the reaction time and enhance the product yield. Despite the high efficiency of *N*-arylation of sulfonamides with copper or palladium as a catalyst with either aryl halides or aryl boronic acids,[43] traditional cross-coupling techniques typically require highly toxic and high-cost heavy transition metals, as well as preactivated coupling partners such as aryl/alkyl halides or pseudo-halides and moisture-sensitive organometallic reagents. Therefore, these techniques often produce undesired, toxic, and stoichiometric side-products.[44] Also, the problem with homogeneous catalysis is the prolonged reaction time and difficulty involved in separating the catalyst from the reaction mixture.[45] To deal with this issue, the development of a recyclable and highly efficient heterogeneous catalyst that would develop the environmental effect of producing *N*-aryl sulfonamide is of much interest and still in high demand. The catalyst is composed of porous crosslinked polysulfonamides which as a non-toxic and biological polymer makes the catalyst more environmentally friendly. Also, as seen in Table 6,

TABLE 6 Comparison of the present methodology with other reported catalysts for the synthesis of 4-methyl-*N*-phenylbenzenesulfonamide 3a

Entry	Conditions	Yield (%) [Ref]
1	CuI(20 mol%), PhI, Ligand, K_3PO_4, DMF, N_2, 100 °C, 48 hr	95[46]
2	CuI(10 mol%), PhBr, MW, K_2CO_3, Ligand, 195 °C, 3 hr	70[28]
3	CuI(20 mol%), PhI, Ligand KF/Al_2O_3, Dioxane, 100–110 °C, 9 hr	93[46]
4	CuI(5 mol%), PhI, Cs_2CO_3, DMF, Air, 130 °C, 24 hr	86[47]
5	CuCl(10 mol%), PhB $(OH)_2$, MeOH, Air, 25 °C, 1 hr	95[43]
6	Pd $(OAc)_2$(20 mol%), PhBr, PEG, TBAA, 35 °C, 4 hr	85[48]
7	PEA-PSA@CuI(3.5mol%), $AgNO_3$(1 mol%), $K_2S_2O_8$, PhCOOH, Toluene, 110 °C, 1 hr	90, 88, 88, 88, 86, 84 [This work]

the presence of crosslinked poly sulfonamides in the support matrix seems absolutely necessary for more chemical stability of catalyst than other ones in the recycled forms because after several runs, whatever the amount of decomposition is less, the activity of the catalyst is surely more. The most significant advantages of this work include high selectivity and efficiency toward the products, experimental simplicity, broad substrate scope, without using base, and using carboxylic acids or inactivated arenes as arylating agents.

4 | CONCLUSIONS

In summary, a novel class of polysulfonamides was synthesized using the template and functionalized monomers and it was then utilized as a stabilizer for the catalytically active CuI NPs. A variety of characterizations confirm that CuI NPs have been successfully grafted on the polysulfonamide surface. The catalytic activity of PEA-PSA@CuI along with silver(I)/persulfate was explored in decarboxylative oxidative C-N coupling of carboxylic acids with sulfonamides to afford *N*-arylsulfonamides, as important materials in medicine and biology. This protocol gave various advantages such as excellent product yields, easy purification, simple procedure, and recyclability of the catalyst. It is expected that the current study can provide the development basis of porous polysulfonamides as tunable support for stabilizing catalytically active species. In conclusion, this article offers a novel application for sulfonamides chemistry.

ACKNOWLEDGEMENTS

The authors would like to thank Bu-Ali Sina University, Center of Excellence Developmental of Environmentally Friendly Methods for Chemical Synthesis (CEDEFMCS) for financial supporting of this research.

ORCID

Sedigheh Alavinia https://orcid.org/0000-0002-5421-777X

Ramin Ghorbani-Vaghei https://orcid.org/0000-0001-8322-6299

Jamshid Rakhtshah https://orcid.org/0000-0002-1421-1007

Jaber Yousefi Seyf https://orcid.org/0000-0001-5624-1127

Iman Ali Arabian https://orcid.org/0000-0002-1970-2358

REFERENCES

[1] B. Aday, H. Pamuk, M. Kaya, F. Sen, *J. Nanosci. Nanotechnol.* **2016**, *16*, 6498.
[2] H. Pamuk, B. Aday, F. Şen, M. Kaya, *RSC Adv.* **2015**, *5*, 49295.
[3] B. Aday, Y. Yıldız, R. Ulus, S. Eriş, M. Kaya, F. Sen, *New J. Chem.* **2016**, *40*, 748.
[4] N. Subhakara reddy, A. Sriniva rao, M. Adharvana chari, V. Ravikumar, V. Jyothy, V. Himabindu, *J. Chem. Sci.* **2012**, *124*, 723.
[5] M. S. Al-Said, M. M. Ghorab, M. S. Al-Dosari, M. M. Hamed, *Eur. J. Med. Chem.* **2011**, *46*, 201.
[6] K. K. Sahu, V. Ravichandran, V. K. Mourya, R. K. Agrawal, *Med. Chem. Res.* **2007**, *15*, 418.
[7] S. More, S. Jadhav, R. Salunkhe, A. Kumbhar, *Mol. Catal.* **2017**, *442*, 126.
[8] J. Yin, S. L. Buchwald, *Org. Lett.* **2000**, *2*, 1101.
[9] J. Cornella, C. Sanchez, D. Banawa, I. Larrosa, *Chem. Commun.* **2009**, *1*, 7176.
[10] P. B. Palde, P. C. Gareiss, B. L. Miller, *J. Am. Chem. Soc.* **2008**, *130*, 9566.
[11] S. Cristol, W. Firth, *J. Org. Chem.* **1961**, *26*, 280.
[12] J. M. Anderson, J. K. Kochi, *J. Am. Chem. Soc.* **1970**, *92*, 1651.
[13] H. Hunsdiecker, C. Hunsdiecker, *Chem. Ges.* **1942**, *75*, 291.
[14] Y. Nakao, *Synthesis* **2011**, *20*, 3209.
[15] F. Fontana, F. Minisci, N. Barbosa, *Tetrahedron* **1990**, *46*, 2525.
[16] F. Minisci, R. Bernardi, F. Bertini, R. Galli, M. Perchinummo, *Tetrahedron* **1971**, *27*, 3575.
[17] G. Fang, X. Cong, G. Zanoni, Q. Liu, X. Bia, *Adv. Synth. Catal.* **2017**, *359*, 1422.
[18] T. Patra, D. Maiti, *Chem. – Eur. J.* **2017**, *23*, 7382.
[19] H. Chechia, L. Yan-Ru, Y. Hung-Chun, *ChemSusChem* **2019**, *12*, 1794.
[20] K. Ganesan, T. Budtova, L. Ratke, P. Gurikov, V. Baudron, I. Preibisch, P. Niemeyer, I. Smirnova, B. Milow, *Materials* **2018**, *11*, 2144.
[21] D. Wu, F. Xu, *Chem. Rev.* **2012**, *112*, 3959.
[22] M. Bailly, M. Kontopoulou, K. Mabrouk, *Polymer* **2010**, *51*, 5506.
[23] Y. Gotoh, R. Igarashi, M. Nagura, Y. Ohkoshi, K. Akamatsu, S. Deki, *J. Mater. Chem.* **2000**, *10*, 2548.
[24] E. Pazos, E. Sleep, C. M. R. Pérez, S. S. Lee, F. Tantakitti, S. I. Stupp, *J. Am. Chem. Soc.* **2016**, *138*, 5507.
[25] R. Ghorbani-Vaghei, N. Sarmast, *Can. J. Chem.* **2017**, *95*, 1073.
[26] D. Azarifar, R. Ghorbani-Vaghei, S. Daliran, A.-R. Oveisi, *Chem. Cat. Chem.* **2017**, *9*, 91992.
[27] a) H. J. Xu, Y. F. Liang, Z. Y. Cai, H. X. Qi, C. Y. Yang, Y. S. Feng, *J. Org. Chem.* **2011**, *76*, 2296; b) H. J. Xu, Y. F. Liang, X. F. Zhou, Y. S. Feng, *Org. Biomol. Chem.* **2012**, *10*, 2562; c) J. Safaei-Ghomi, A. Ziarati, R. Teymuri, *Bull. Korean Chem. Soc.* **2012**, *33*, 2679; d) S. Abdolmohammadi, M. Afsharpour, *Z. Naturforsch.* **2015**, *70b*, 171; e) S. Abdolmohammadi, Z. Aghaei-Meybodi, *Comb. Chem. High T. Scr.* **2015**, *18*, 911; f) S. Abdolmohammadi, R. Ghiasi, S. Ahmadzadeh-Vatani, *Z. Naturforsch.* **2016**, *71b*, 777; g) S. Abdolmohammadi, S. Karimpour, *Chin. Chem. Lett.* **2016**, *27*, 114; h) S. Abdolmohammadi, S. Dahi-Azar, M. Mohammadnejad, A. Hosseinian, *Comb. Chem. High T. Scr.* **2017**, *20*, 773.
[28] H. He, Y.-J. Wu, *Tetrahedron Lett.* **2003**, *44*, 3385.
[29] J. Baffoe, M. Y. Hoe, B. Touré, *Org. Lett.* **2010**, *12*, 1532.
[30] a) H. Veisi, R. Ghorbani-Vaghei, S. Hemmati, M. H. Aliani, T. Ozturk, *Appl. Organomet. Chem.* **2015**, *29*, 26; b) R. Ghorbani-Vaghei, S. Alavinia, N. Sarmast, *Appl. Organomet.*

Chem. **2018**, *32*, e4038; c) R. Ghorbani-Vaghei, S. Alavinia, Z. Merati, V. Izadkhah, *Appl. Organomet. Chem.* **2018**, *32*, e4127.
[31] R. Ghorbani-Vaghei, H. Jalili, *Synthesis* **2005**, *7*, 1099.
[32] W. Stöberand, A. Fink, *J. Colloid Interface Sci.* **1968**, *26*, 62.
[33] J. Safaei-Ghomi, S. Rohani, A. Ziarati, *J. Nanostruct.* **2012**, *2*, 79.
[34] M. Khalaj, M. Ghazanfarpour-Darjani, M.-R. Talei, B. Olyai, S. Faraji Shamami, *J. Sulfur Chem.* **2016**, *37*, 211.
[35] J. Lin, H. Huang, M. Wang, J. Deng, *Polym. Chem.* **2016**, *7*, 1675.
[36] S. Belali, R. Karimi, M. Hadizadeh, *Polymer* **2017**, *109*, 93.
[37] D. Campbell, S. M. Carnell, R. J. Eden, *Eye & Contact Lens.* **2013**, *39*, 254.
[38] S. W. Sing, W. Kenneth, *Ads. Sci. Tech.* **2004**, *22*, 773.
[39] X. F. Wang, Y. H. Shen, A. J. Xie, *J. Mater. Chem.* **2011**, *21*, 9641.
[40] S. Li, Y. Li, J. Cao, J. Zhu, L. Fan, X. Li, *Anal. Chem.* **2014**, *86*, 10201.
[41] J. A. McMillan, *Chem. Rev.* **1962**, *62*, 65.
[42] a) W.-P. Mai, G. Song, G.-C. Sun, *RSC Adv.* **2013**, *3*, 19264; b) E. Sperotto, G. P. M. van Klink, G. van Koten, J. G. de Vries, *Dalton Trans.* **2010**, *39*, 10338.
[43] A. d. Meijere, F. Diederich (Eds), *Metal-Catalyzed Cross-Coupling Reactions*, Vol. 1 and 2, Wiley-VCH Verlag GmbH, Weinheim **2008** 891.
[44] S.-Y. Moon, J. Nam, K. Rathwell, W. Kim, *Org. Lett.* **2014**, *16*, 338.
[45] L. Chip, Q. Chen, T. Liang, P. Zhang, D. MacMillan, *Org. Chem.* **2018**, *360*, 1010.
[46] W. Deng, L. Liu, C. Zhang, M. Liu, Q. Guo, *Tetrahedron Lett.* **2005**, *46*, 7295.
[47] R. Hosseinzadeh, M. Tajbakhsh, M. Mohadjerani, M. Alikarami, *J. Chem. Sci.* **2010**, *122*, 143.
[48] Y.-C. Teo, F.-F. Yong, *Synlett* **2011**, *6*, 837.

SUPPORTING INFORMATION

Additional supporting information may be found online in the Supporting Information section at the end of this article.

How to cite this article: Alavinia S, Ghorbani-Vaghei R, Rakhtshah J, Yousefi Seyf J, Ali Arabian I. Copper iodide nanoparticles-decorated porous polysulfonamide gel: As effective catalyst for decarboxylative synthesis of *N*-Arylsulfonamides. *Appl Organometal Chem*. 2020; e5449. https://doi.org/10.1002/aoc.5449